Article

# Single-chip silicon photonic engine for analog optical and microwave signals processing

Hong Deng [1,2] ✉, Jing Zhang[1,2], Emadreza Soltanian [1,2], Xiangfeng Chen[1,2], Chao Pang[1,2], Nicolas Vaissiere [3], Delphine Neel[3], Joan Ramirez[3], Jean Decobert[3], Nishant Singh [4], Guy Torfs[4], Gunther Roelkens[1,2] & Wim Bogaerts [1,2] ✉

We present a photonic engine that processes both optical and microwave signals, and can convert signals between the two domains. Our photonic chip, fabricated in IMEC's iSiPP50G silicon photonics process, is capable of both generation and detection of analog electrical and optical signals, and can program user-defined filter responses in both domains. This single chip integrates all essential photonic integrated components like modulators, optical filters, and photodetectors, as well as tunable lasers enabled by transfer-printed indium phosphide optical amplifiers. This makes it possible to operate the chip as a black-box microwave photonics processor, where the user can process high-frequency microwave signals without being exposed to inner optical operation of the chip. The system's configuration is locally programmed through thermo-optic phase shifters and monitored by photo-detectors, and can select any combination of optical or microwave inputs and outputs. We construct multiple systems with this engine to demonstrate its capabilities for different RF and optical signal processing functions, including optical and RF signal generation and filtering. This represents a key step towards compact and affordable microwave photonic systems that can enable higher-speed wireless communication networks and low-cost microwave sensing applications.

Modern communication networks rely on the convergence of high-speed fiber-optic landlines and wireless radio-frequency (RF) microwave communications. The relentless expansion of these networks demands enhanced granularity, heightened data transmission, and operation at ever-higher frequency bands. Facilitating this exponential growth requires network nodes that can process both optical and microwave signals, convert between these domains, and, most importantly, have a reduced footprint, power consumption, and cost. In this quest, microwave photonics (MWP) emerges as a promising frontier, leveraging the vast bandwidth capabilities of optics to undertake signal processing tasks within the optical domain. Despite this potential, prevalent MWP demonstrations have predominantly relied on costly, power-intensive fiber-based systems that exhibit limited scalability[1-3]. Furthermore, earlier efforts at integrating on-chip systems have faced limitations, providing a limited subset of the necessary functionalities, or necessitating the use of several off-chip devices to achieve the intended capabilities[4-8].

[1]Photonics Research Group, Department of Information Technology, Ghent University - imec, Ghent, Belgium. [2]Center for Nano- and Biophotonics (NB Photonics), Ghent University, Ghent, Belgium. [3]III-V Lab, a joint venture by Nokia, Thales and CEA, Palaiseau, France. [4]IDLab, Department of Information Technology, Ghent University - imec, Ghent, Belgium. ✉e-mail: hong.deng@ugent.be; wim.bogaerts@ugent.be
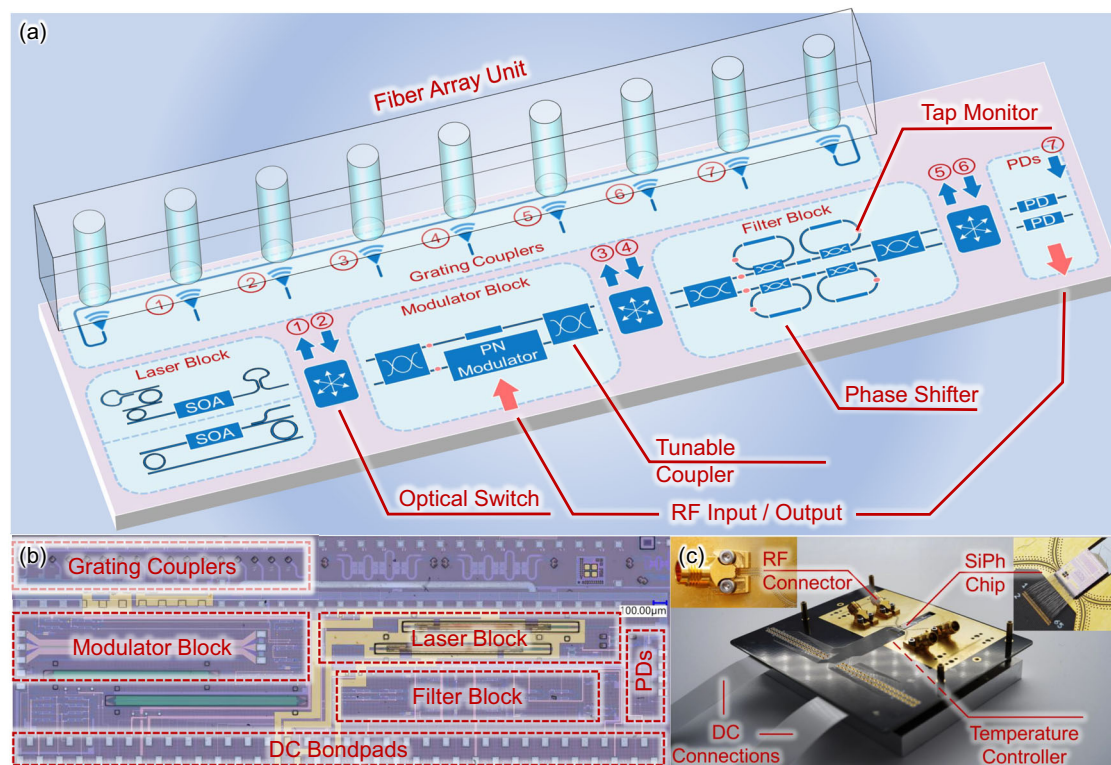
**Fig. 1 | Silicon photonic engine: design, fabrication, and packaging. a** Schematic block diagram of the silicon photonic engine. **b** Microscope image of the fabricated chip; **c** A packaged demonstrator with wirebonded controls and microwave connectors (before fiber attachment).

We present a key breakthrough in this paper, demonstrating a self-contained silicon photonic engine that can process both optical and microwave signals, and can convert signals between the two domains. This chip, which combines lasers, high-speed electro-optic modulators and detectors, and a programmable optical filter, can be considered the first demonstration of a full black-box microwave photonics process engine: for a user who wants to process analog RF signals, the internal optics of the chip are hidden. The signals going in and out can be confined to the RF domain, and no optical connections or external optical devices are essential for the operation.

However, we conceived our chip with more diverse functionality in mind, providing full programmability of the internal signal flow, such that the chip can be used with any combination of optical and microwave input and output signals. Equipped with optical connections and supporting devices, our photonic chip can be used not only for simple functions such as a tunable light source or a photodetector, but also as a high-speed transmitter or receiver, a tunable optical or microwave filter, a frequency converter, or a tunable opto-electronic oscillator (OEO). The programmability of our chip guarantees its robust performance, and control and calibration of the entire chip can be executed entirely in the electrical domain, using optical monitors strategically placed throughout the chip. This makes the chip a flexible engine that can be used to construct different microwave photonic systems.

To realize this integration of functions, we built on the standard iSiPP50G silicon photonics platform from *imec*[9]. This platform provides almost all key functions expected from silicon photonics, including low-loss waveguides and passive components, high-speed modulators and detectors, and thermo-optic phase shifters to tune the optical response. The key missing on-chip component in this platform is the light source: for this, we used micro-transfer-printing to integrate indium phosphide (InP) optical amplifier[10]. Combined with the on-chip tunable filter circuits, they can function as a widely tunable laser[11]. Optical signals can be coupled to and from optical fibers through grating couplers[12]. High-speed RF signals can be fed into electro-optic modulators, who imprint this RF signal onto an optical carrier wavelength generated by the on-chip laser. These optical signals can then be processed on-chip by a tunable optical filter bank, and converted again to the RF domain through high-speed photodetectors.

Our full integration approach also enables an entirely new way to treat microwave signals in the optical domain. The common approach is to employ single-sideband modulation, where half of the modulated signal is discarded, introducing inherent end-to-end system losses[4,5]. In our approach, we designed a reconfigurable modulator subcircuit that gives us arbitrary control over the phase relation between the sidebands and the optical carrier, and our optical filter block allows us to independently filter them before converting them back to the RF domain in the photodetector. This new formalism of signal processing does not suffer from the inherent loss of single-sideband modulation, but also simplifies the filter design algorithms.

Figure 1 shows the silicon photonics chip and its corresponding block diagram. The signal pipeline runs from the tunable lasers through the modulators (where the RF signal comes in) over the filter bank to the photodetectors to the RF output bondpads. All elements on the chip are fully tunable with on-chip thermo-optic phase shifters. And to allow arbitrary use of both optical and microwave signals, we introduced optical switches between the individual blocks in the system that interface with optical fibers, allowing the user to inject or extract light at every stage of the flow, and even create fiber-based feedback loops, as we will demonstrate further.

To demonstrate the versatility of our silicon photonic engine, we demonstrate different optical and electrical functions: optical-to-electrical signal conversion and the reverse operation, optical and microwave filtering and equalization, and microwave frequency doubling. We also combine our chip engine with a fiber loop to implement a tunable opto-electronic oscillator (OEO). The details of these different demonstrations are described in the supplementary material. Additional applications, including but not limited to radio over fiber
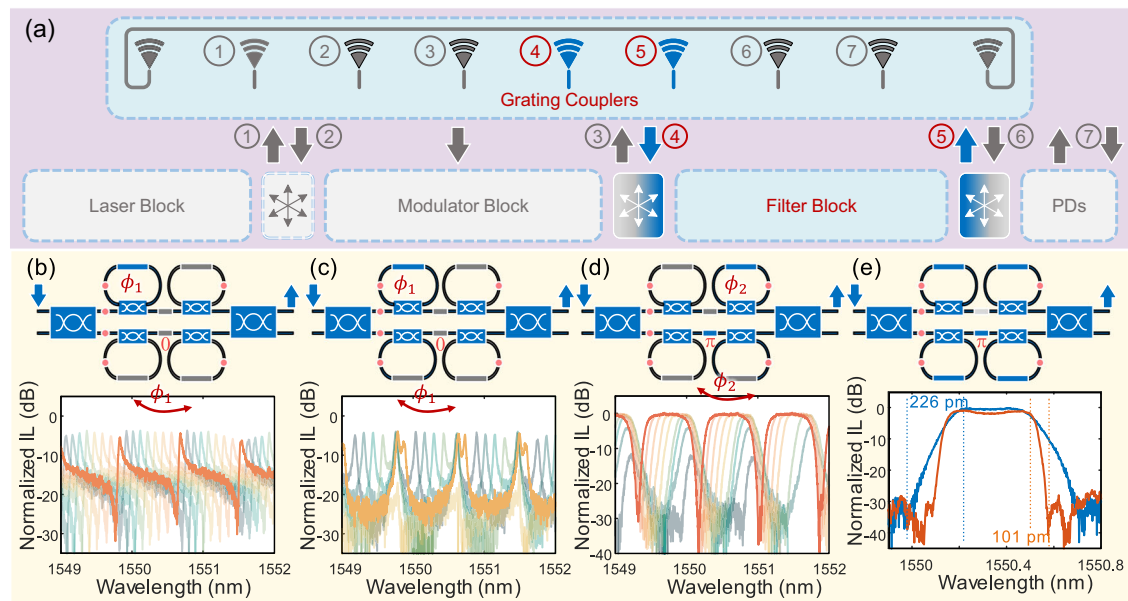
**Fig. 2 | Characterization of optical filtering responses. a** The processing engine configuration for optical filtering. **b** Single bandpass filtering configuration and response. One upper ring is used, the phase shifter is set to 0; **c** Double bandpass filtering configuration and response. One upper ring and one lower ring are used; the phase shifter is set to 0; **d** Second-order Chebyshev Type II bandpass filtering configuration and response, one upper ring and one lower ring are used, phase shifter is set to $\pi$; **e** Fourth-order Chebyshev Type II bandpass filtering configuration and response. Four rings are used, phase shifter is set to $\pi$.

links[13], RF instantaneous frequency measuring[14], RF phase tuning[15], signal temporal computing[8,16], optical and RF switching, and optical sensing[17] and interrogation[18], can clearly be realized with our photonic engine, though we will not discuss all these possibilities in this paper.

## Results

Our photonic chip consists of four main blocks, which are a tunable laser block (with 2 lasers), a reconfigurable modulator block, a reconfigurable optical filter block, and a high-speed PD block, as shown in Fig. 1a. The longest on-chip optical path starts with light generated by the laser source(s), which is then guided into the modulator circuit, which can be configured for RF signal phase modulation, intensity modulation, or its combination, by tuning the embedded static phase shifters (details in the Supplementary Information 3.3). The light, now modulated with an RF payload signal, will be fed into the optical filter block, which consists of a fully tunable four-ring-loaded MZI with tap monitors. The filtered light signal is then converted back into the RF domain by the high-speed PD. The four functional blocks are connected by optical switches, making it possible to inject or extract light signals from outside at each joint, allowing the chip configurations for both optical and RF signal processing, or cascading of these chips through fiber links. The optical switches are implemented as single-stage or double-stage MZIs, tuning with optical phase shifters and monitoring with tap monitors (details in Supplementary Information 3.2)[19]. A fabricated chip is shown in Fig. 1b, and a packaged device (before fiber attachment) is shown in Fig. 1c. The entire photonic circuit has 15 optical fiber ports, 1 RF input and 2 RF outputs, 52 heater-based optical phase shifters, and 8 tap monitors. It has the capability of fully reconfiguring the optical and electrical response and the conversions between the domains, and it can also function as a tunable laser source or a tunable RF source.

### Optical-to-optical (O/O) response

Figure 2 pictures the process engine configured as an optical linear filter: The light signal is guided through the MZI loaded with four independently tunable ring resonators (two in each arm). Such ring-loaded MZIs can act as an auto-regression/moving average (ARMA) filter[4,20,21]. We implemented all couplers in the filter as tunable MZIs, as

shown in Fig 2b–e. With the built-in tap monitors, the coupling status of each ring can be calibrated locally. The tuning procedures are explained in the Supplementary Information 2.4. The optical responses shown in Fig. 2b–e are measured with an optical vector analyzer (LUNA OVA5000) and normalized to the grating coupler transmission envelope. If the phase difference in the MZI is zero, the rings will introduce sharp pass bands as shown in Fig. 2b, c. The fabricated rings show a 3 dB bandwidth of 35 pm when critically coupled. If the MZI phase difference is set to $\pi$, an overcoupled ring pair can form typical Chebyshev Type II filters with a flat passband. The measurements show passbands with ~ 0.5 dB ripple in passbands and 30 dB stopbands rejection (Fig. 2d). By the tuning the second ring pair to the roll-off points, a higher-order Chebyshev Type II filter response is obtained, improving the roll-off bandwidth from 226 pm to 101 pm (Fig. 2e). More details and examples of optical filtering are described in the Supplementary Information 3.4.

### Electrical-to-optical (E/O) response

Combining the laser(s) and modulator, we can imprint RF signals onto the optical carrier(s), corresponding to a pure electrical-to-optical response, as shown in Fig. 3. The on-chip tunable lasers consist of a Fabry-Pérot (FP) laser and a ring laser with intra-cavity wavelength filters. The measurements show -3 dBm optical power coupled to fiber with a tuning range of 60 nm. Depending on the design of the transfer-printed SOA, the lasing range can be adjusted[11] (details in Supplementary Information 3.1). The reconfigurable modulator block consists of a Mach-Zehnder modulator with tunable couplers and a PN junction carrier depletion modulator in one arm, and a slow thermal phase shifter in the other arm. With the tunable couplers and phase shifter, we can configure the modulator to provide either an intensity modulation or pure phase modulation[22] (details in Supplementary Information 3.3). The measurement setup is shown in Fig. 3b. Figure 3c shows the E/O response of the modulator block setting for intensity modulation and pure phase modulation. It exhibits more than 20 dB extinction with the same optical powers in an off-chip PD. When equalized by the filter block (discussed later), the 3 dB bandwidth of the packaged system can be improved from 4.5 GHz to 26 GHz without any pre-calibration (details in Supplementary Information 4.1).
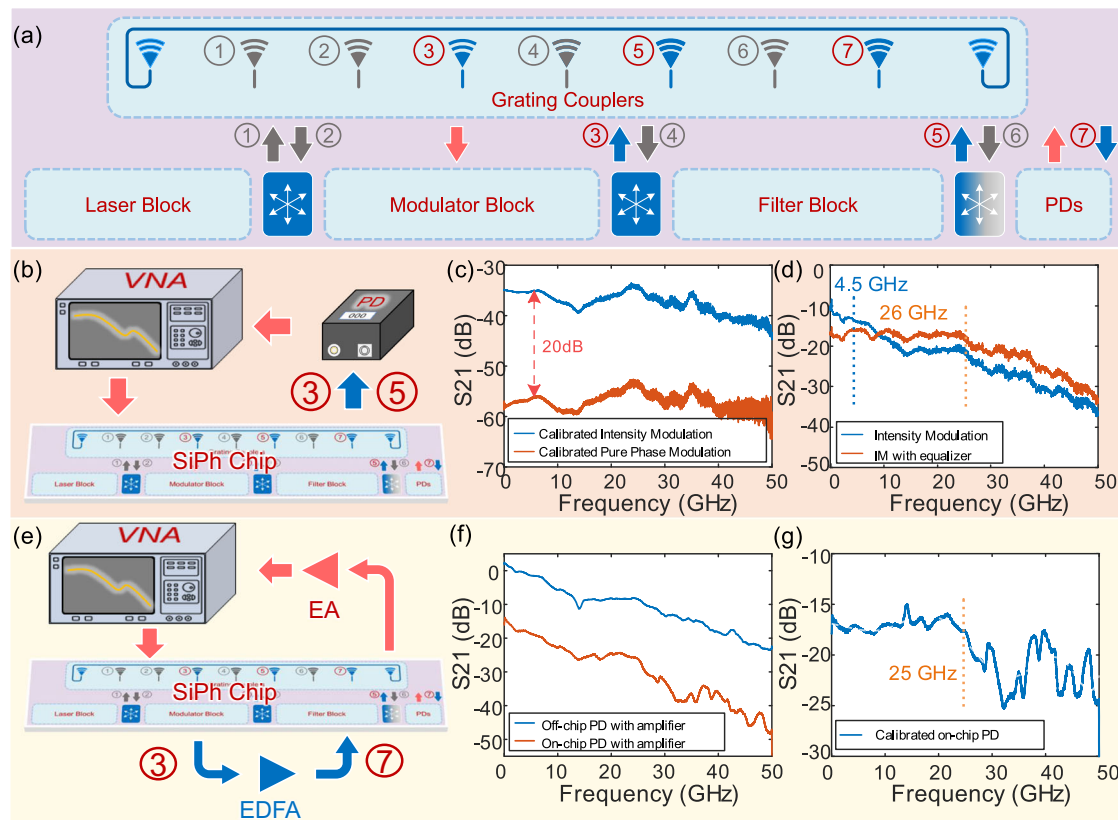
**Fig. 3 | Characterization of E/O and O/E conversion responses. a** The engine configuration for E/O conversion and O/E conversion. **b** The measurement setup for the E/O response characterization; **c** The E/O response of the modulator's intensity modulation and pure phase modulation; **d** The E/O response of an equalized intensity modulation; **e** The measurement setup for the O/E response characterization; **f** The O/E response with off-chip PD and on-chip PD; **g** Calibrated on-chip PD response. VNA Vector Network Analyzer, EA Electronic Amplifier, EDFA Erbium-Doped Fiber Amplifier.

## Optical-to-Electrical (O/E) response

The O/E conversion is implemented by two on-chip PDs. The characterization setup is shown in Fig. 3e. Because the packaged connectors of the packaged chip still introduce excessive RF crosstalk, we make use of our engine's optical ports to integrate an extra erbium-doped fiber amplifier (EDFA) in the signal path. This boosts the modulated light signal, in turn enhancing the electrical signal. The system response is measured both with an off-chip PD and an on-chip PD, shown in Fig. 3f. Taking the off-chip PD as a reference, the O/E response of the on-chip PD shows a 3 dB bandwidth of 25 GHz, as shown in Fig. 3g. More details are shown in the Supplementary Information 3.5.

## Electrical-to-electrical (E/E) response

The packaged chip can act as an analog microwave processor and implement sophisticated linear filtering of RF signals, as shown in Fig. 4. For characterization, the response is measured with an off-chip PD avoid the RF crosstalk altogether. Unlike previously demonstrated integrated microwave photonic filters using single-sideband modulation (SSB)[4,5], our processing engine can use both modulated sidebands, which simplifies the optical filter design. The reconfigurable modulator can generate sidebands with a tunable phase relationship (details in Supplementary Information 3.3), and with the reconfigurable optical filters, the RF response coming from the PDs can be achieved by controlling the interference between the upper and lower RF sidebands. Furthermore, to construct a generalized bandpass or band-stop filter in the RF domain, our approach requires a simple cascade of ring filters that can be independently tuned. More details explaining the unique benefits of this double-sideband approach can be found in Supplementary Information 4.1. Figure 4b–g shows various

types of RF filter responses, realized by tuning both the modulator block and the rings. With a limited on-chip laser power, the whole RF gain of our chip is limited to −35 dB, and the noise figure is limited to 53 dB. Limited by the Q factors of the rings, the narrowest 3 dB RF filter bandwidth is ~ 3 GHz. More details are shown in Supplementary 4.1.

## RF frequency multiplier

Our signal processing engine can implement RF frequency doubling using the laser, the modulator and the detector, as shown in Fig. 5a. Fig. 5b shows a measurement setup for the nonlinear RF responses. By biasing the Mach-Zehnder modulator at its null point[23], the ratio of the second-harmonic signal ($2f$) to the linear response ($1f$) can be adjusted by tuning the couplers in the modulator block such that the losses in both arms are fully balanced (this is a 70:30 balance as the PN modulator has a higher loss, as shown in Fig. 5c). The frequency doubling results with the off-chip PD and on-chip PD are shown in Fig. 5d and e, respectively. The results show that the $2f/1f$ signal ratio is as high as 40 dB with off-chip PD. For an on-chip PD, the RF crosstalk degrades the $1f$ extinction (details in Supplementary Information 4.2).

## Opto-electronic oscillator (OEO)

We can also use our signal processing engine to construct more sophisticated functions. For instance, by connecting an external PD, additional amplifiers (to compensate the loss in the RF bandpass filters shown above) and a long fiber delay line, our engine can now act as an OEO with a tunable central frequency, as shown in Fig. 6. The fiber creates a much longer longer oscillation cavity, which is indicated in Fig. 6b. With this system, RF signals can be generated with a frequency tunable from 4 GHz to 24 GHz and −116 dBc/Hz phase noise at 100 kHz offset frequency, shown in Fig. 6c. And with the on-chip PD, the
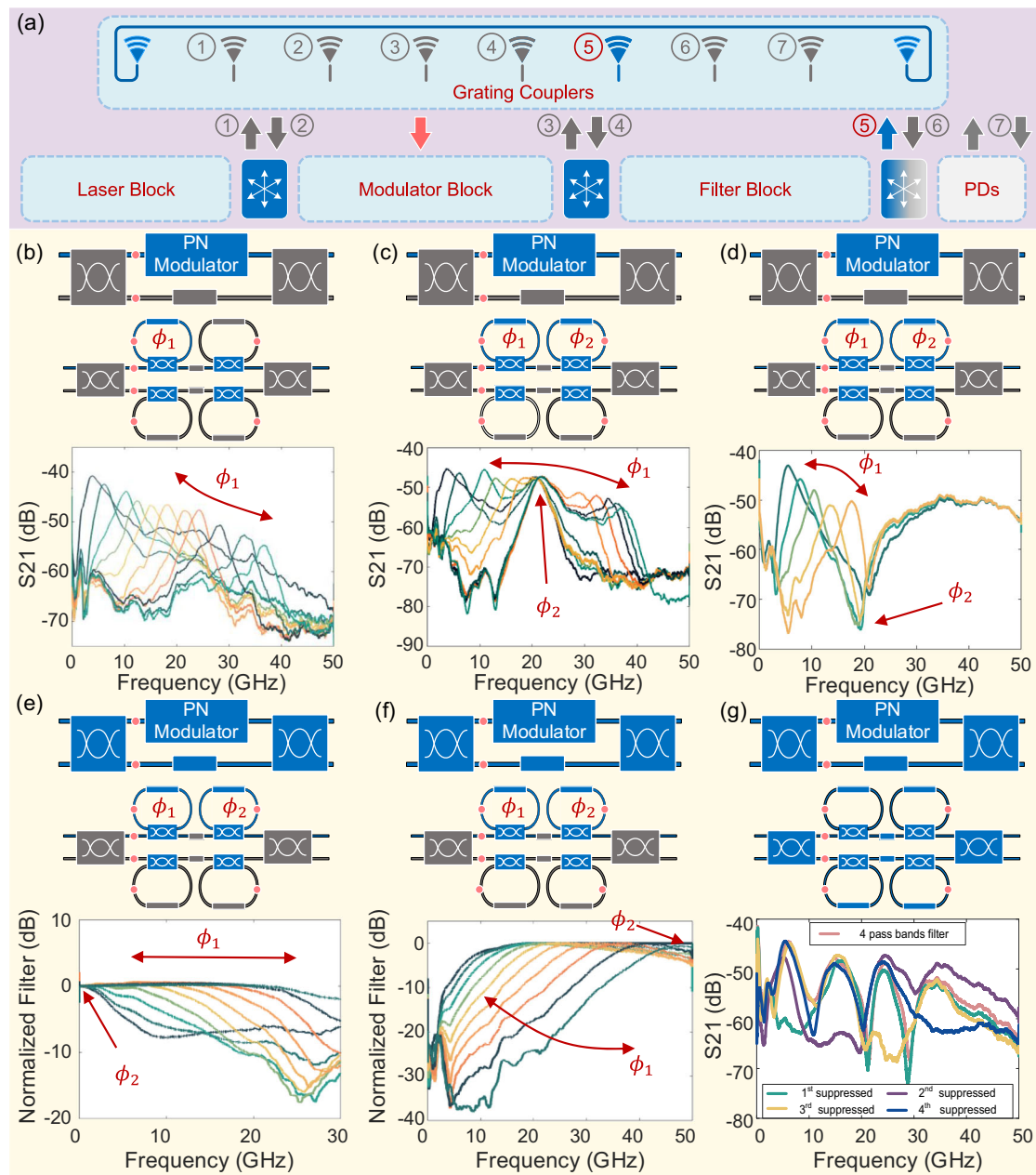
**Fig. 4 | Characterization of microwave photonic filtering responses. a** The engine configuration for E/E conversion. **b** Microwave filter: single tunable bandpass filter. **c** Microwave filter: double tunable bandpass filter; **d** Microwave filter: tunable one-pass one-stop band filter; **e** Microwave filter: tunable low pass filter; **f** Microwave filter: tunable high pass filter, **g** Microwave filter: four tunable bandpass filters.

generated signal can be tuned from 3.3 GHz to 11.6 GHz with −84 dBc/Hz phase noise at 100 kHz offset frequency, shown in Fig. 6d. More details are shown in Supplementary Information 4.3.

Except for the functionalities shown above, our signal processing engine can also work as an optical wavelength meter or RF frequency meter using the tap monitors in the filter block, where the resolution is limited by the $Q$ factor of the loaded ring (Supplementary Information 4.4).

## Discussion
### System integration, flexibility and performance evaluation
Our single-chip signal process engine, with a footprint of only 5 mm × 1.3 mm (not including the grating coupler array), provides a fully programmable filtering response for both optical and RF signals, as well as generation and detection of electrical and optical signals.

This is a very complete set of functions typically needed in microwave photonics systems. For comparison, an overview of recent progress in the integrated photonic signal processor is shown in Table 1, based on a similar table in Ref. 4. To the best of our understanding, our engine represents a pioneering demonstration on a silicon photonic platform, achieving a seamless integration of all essential components. These components are interconnected with optical switches. By adjusting these switches, our photonic engine can perform a wide range of functions and serve as a critical building block in optical and micro-wave systems. To the best of our awareness, it also stands as a groundbreaking demonstrator showcasing such an extensive level of programmability.

Utilizing micro-transfer printing technology, we successfully integrated two tunable laser sources heterogeneously into our photonic engine. By employing different SOA coupons, the laser sources
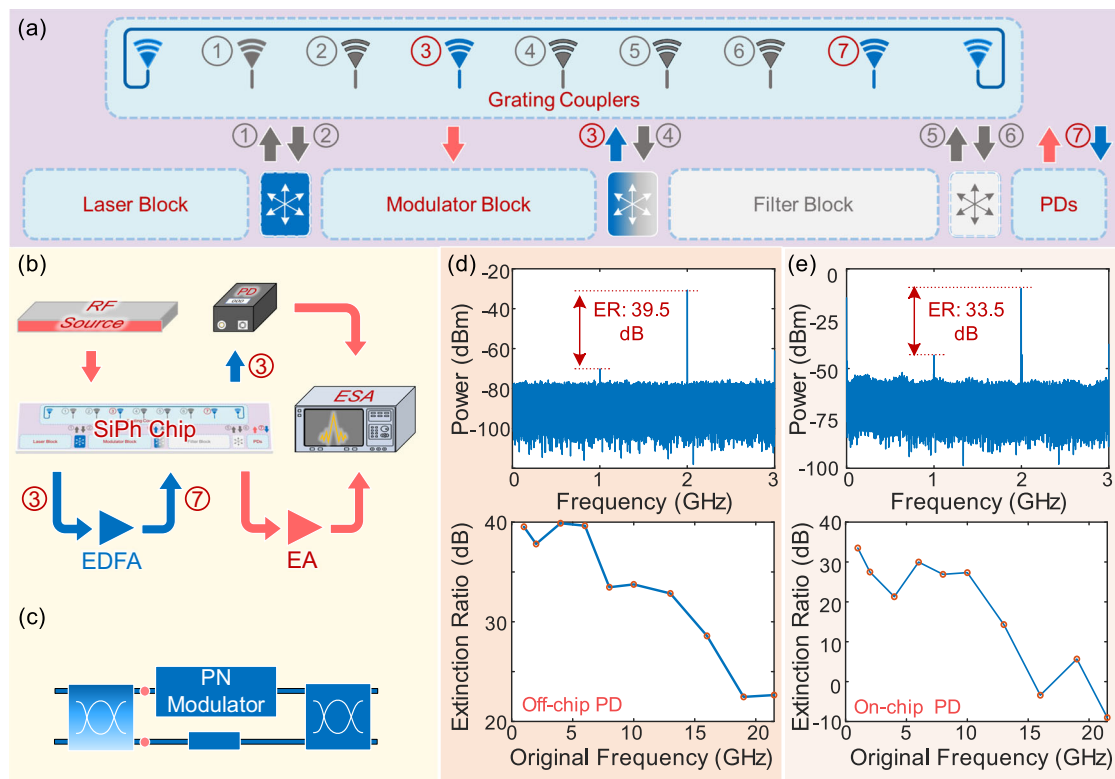
**Fig. 5 | Characterization of Frequency Doubling Responses. a** The engine configuration for RF frequency doubling. **b** Measurement setup for the nonlinear RF responses. **c** Configuration of the modulator block for high extinction ratio; **d** Frequency doubling results with off-chip PD; **e** Frequency doubling results with on-chip PD. EA Electronic Amplifier, EDFA Erbium-Doped Fiber Amplifier, ESA Electrical Spectrum Analyzer.

together achieve an approximate tuning range of 90 nm with a peak off-chip power of -3.5 dBm (-8 dBm as reported in Ref. 4).

Beyond the photonic chip, we implemented thoughtful packaging, ensuring high robustness. Still, even with state-of-the-art isolation (60 dB, compared to less than 20 dB in Ref. 4) between the RF input and output ports, the packaged engine still suffers from significant RF crosstalk. (details can be found in Supplementary Information 2). Even with those limitations, it shows a good overall performance compared to other demonstrations. e.g. the bandwidth of modulator (our work 34 GHz with a second-degree polynomial fit, 5 GHz in Ref. [4], 15 GHz in Ref. 7,5.4 GHz in Ref. 24), optical filters' FSR (107 GHz in our work, 20 GHz in Refs. 4 and[25], 50 GHz in Ref. 5,55 GHz in Ref. 26), and filter's narrowest bandwidth(4 GHz in our work, 6 GHz in Ref. 4,5 GHz in Ref. 26). Its application demonstrators also show excellent results, like the tunable OEO's large frequency tuning range (larger than 24 GHz in our work, maximum 7 GHz in Ref. 27, fixed 10 GHz in Ref. 6) and lower phase noise than commercial RF sources. When programmed as a microwave photonic link, our photonic engine shows a RF gain of −35 dB (similar to −36.98 dB in Ref. 28), a noise figure of 53.5 dB (42.19 dB in Ref. 28), and a SFDR of 107 dBHz$^{2/3}$. More details are shown in Supplementary Information 4.1.

In-line PD monitors in our photonic engine are included to calibrate and configure our photonic engines without using external optical devices. Furthermore, thanks to its high flexibility, our photonic engine can be combined with specialized off-chip devices to construct larger systems, or improve its performance where needed.

**Microwave photonic filtering based on dual-sideband modulation**

The E/E response of the processing engine is based on dual-sideband modulation. Compared to SSB modulation schemes in other works[4,5,26,29], our algorithm enables a much simpler filter design and

configuration, and it has a lower intrinsic RF loss. The commonly used SSB modulation scheme for arbitrary RF filtering requires filtering out one sideband of the RF-modulated signal, throwing away half of the modulated signal. Even in an ideal case, this results in an intrinsic 3 dB RF loss. Also, the SSB scheme maps an arbitrary optical filter into the RF domain, which typically necessitates a ring-loaded Mach-Zehnder interferometer (MZI).

In contrast, our chip is based on a double-sideband modulation scheme, keeping all the modulated RF power, as it eliminates the need for an additional optical filter for SSB suppression, saving at least 3 dB in both optical and RF power. In addition, we can perform arbitrary RF filtering only cascaded all-pass filters. In our demonstrations, we used two cascaded ring filters to achieve the RF filtering shapes shown in Fig. 4. The cascaded ring filter and its tuning process are also significantly simpler than the ring-loaded MZI used in other works. In addition, the reconfigurable modulator, with tunable splitter and combiner, ensures the minimum optical loss in all scenarios.

**Optical switches performance**

The configurability of our photonic engine depends on the tuning of the optical switches. Because of the nature of optical interference, even minor light crosstalk in a coherent system can significantly impair the performance[30]. To address this, our photonic engine employs optical switches for coherent optical splitting and combining that are built with double-stage MZI structures. The coupling in these switch circuits can be tuned from 0 to 1 and are highly tolerant of directional coupler fabrication errors[19]. Our measurements show that these optical switches can achieve extinction ratios of 40 dB (further details can be found in Supplementary Information 3.2). As these switches are somewhat more difficult to address (due to the additional tuning elements), we have included sufficient in-line photodiode (PD) monitors to calibrate and configure them.
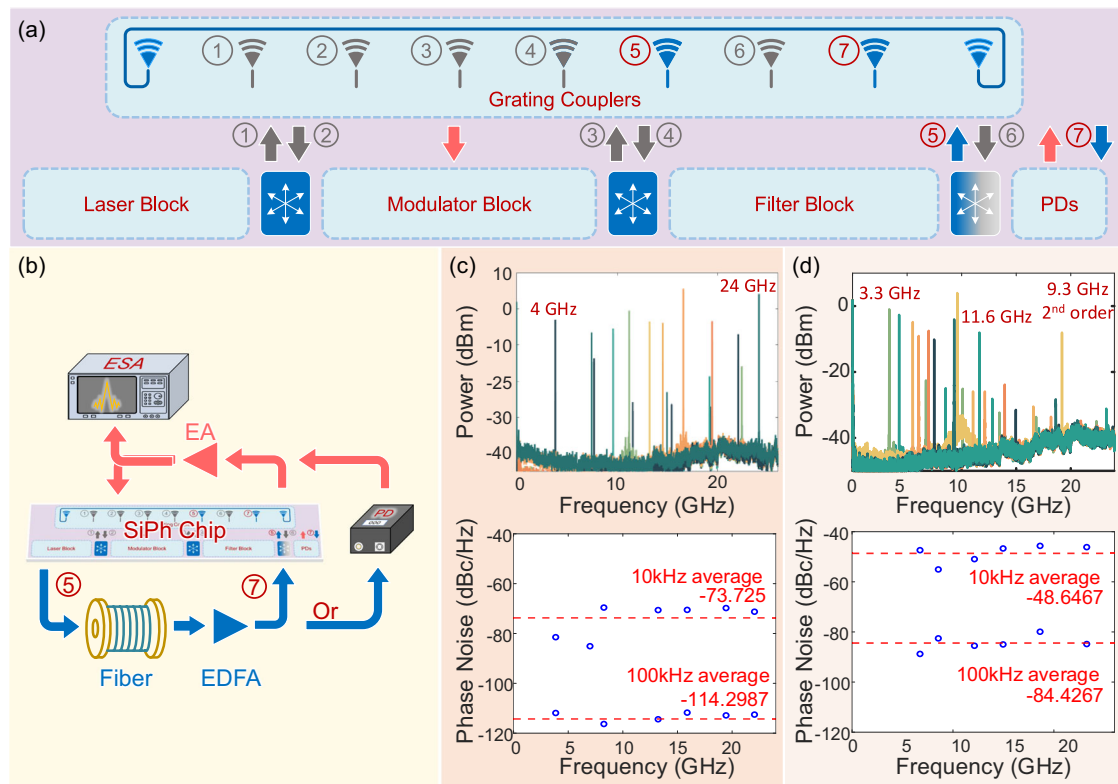
**Fig. 6 | Characterization of an opto-electronic oscillator response. a** The engine as the heart of an opto-electronic oscillator. **b** Measurement setup for the OEO. **c** RF signal generation with 500 m fiber and off-chip PD; **d** RF signal generation with 20 m fiber and on-chip PD; ESA Electrical Spectrum Analyzer, EA Electronic Amplifier, EDFA Erbium-Doped Fiber Amplifier.

**Table 1 | Comparison of recently published integrated microwave photonic systems**

| Year | Reference | Functionality | platform | Components | | | | |
|------|-----------|---------------|----------|---|---|---|---|---|
| | | | | a | b | c | d | e |
| 2016 | 16 | Multiple | InGaAsP/InP | off | - | off | on | off |
| 2016 | 4 | Filter | InGaAsP/InP | on | on | on | on | on |
| 2018 | 27 | OEO | SOI | off | - | on | on | on |
| 2020 | 32 | Multiple | SOI | off | - | off | on | off |
| 2021 | 5 | Filter | SOI | off | - | off | on | on |
| 2021 | 28 | TTD | InP + SiN | on | on | on | - | on |
| 2021 | 25 | Multiple | SiN | off | off | off | on | off |
| 2022 | 33 | TTD | SOI | off | - | off | on | off |
| 2022 | 29 | Filter | SOI | off | - | off | on | off |
| 2023 | 7 | Filter | SOI | off | on | on | on | on |
| 2023 | 26 | Filter | SOI | off | - | off | on | off |
| 2024 | 6 | Multiple | SOI | off | - | off | on | off |
| 2024 | 24 | BSS | SOI | off | - | on | on | on |
| 2024 | 8 | TC | LNOI | off | - | on | on | off |
| 2023 | This work | Multiple | SOI | on | on | on | on | on |

*OEO* Opto-electronic oscillator, *TTD* True time delay, *BSS* blind source separation, *TC* temporal computing, a: optical source; b: reconfigurable optical source shaping system; c: optical modulator; d: reconfigurable optical filtering system; e: photodetector.

## Filtering performance and scale-up analysis

The optical and electrical filters are both based on the same optical filter block in our processing engine. As a tunable filter, the minimum 3 dB bandwidth depends on the quality ($Q$) factor of the ring resonators, which are ~50,000 at critical coupling. The monitor PDs inside the ring introduce some extra loss (limiting the $Q$), but they allow us to directly monitor the ring status for configuration. Better calibration schemes or a tunable power tap should allow us to reduce the impact of these monitor PDs.

The filtering performance is also limited by the filter order, which corresponds to the number of ring resonators in the block. For a higher-order RF filter, we only need to cascade additional rings, which is very scalable in terms of optical losses and tuning scheme. For optical filtering, increasing the order requires extra ring pairs over both arms of the MZI.

## Equalized E/O conversion with widely tunable optical carriers

The two on-chip laser sources both show 50 nm tuning ranges in different wavelength regions, and a total 90 nm tuning range (from 1508 nm to 1598 nm). With the on-chip modulators, an E/O conversion with widely tunable optical carriers can be reached.

The programmable filter can also be used as an RF equalizer. In the Supplementary Information 4.2 we show how we compensate the uneven RF loss of the PCB and bonding wires, boosting the 3 dB bandwidth from 4.5 GHz to 26 GHz.

In addition, the on-chip laser together with two PDs can also be configured as a coherent receiver with tunable local oscillator (LO). But due to the high RF crosstalk (discussed in the crosstalk section), we did not further evaluated this.

## Laser generation

We used micro-transfer-printing technology to integrate two tunable lasers into our photonic engine. These tunable lasers cover a wavelength range from 1507 nm to 1575 nm, with a maximum output power of -3 dBm (measured at the output fiber) and an intrinsic linewidth of 45 kHz. All demonstrations in this work are based on these two on-chip

lasers. Additional details are provided in Supplementary Information 3.1 and in Ref. 10.

For optical signal filtering and detection, the performance of the on-chip laser does not significantly affect the results. However, for microwave photonic applications, the on-chip laser performance is critical. First, the laser output power directly influences the RF gain of the system, especially when no additional optical amplification is used-higher laser power enhances the overall system gain. Second, the phase noise of the on-chip laser contributes to the accumulated phase noise of the signal within the system. Therefore, minimizing laser phase noise is essential for maintaining high signal integrity and overall system performance.

### RF signal generation

We reported two demonstrations of how we can use our engine to build RF signal generators. We showed frequency doubling with 40 dB $2f/1f$ extinction ratio using the configurable modulator, and a tunable opto-electronic oscillator (OEO) when combining the engine with an external fiber and RF amplifier. The OEO's RF generation covers the 4-24 GHz span with almost constant phase noise of -114 dBc/Hz at 100 kHz using an off-chip PD. This is superior to commercial products (R&S SMR, -105 dBc/Hz at 100 kHz offset frequency for 10 GHz central frequency). The frequency generation of the OEO system is not limited to 24 GHz with our process engine, but its phase noise measurement is limited by the used spectrum analyzer (26 GHz).

### Power consumption

The energy usage of our photonic engine is contingent on the number of functional blocks employed. Our system contains two lasers, one modulator, and around 52 phase shifters (each tunable coupler contains two phase shifter). To fully operate the system, we will need to drive one laser, the modulator, and 23 phase shifters, including 17 tunable couplers (only one arm driven is needed for each tunable coupler), and 6 phase shifters for offset phases. The transfer-printed laser unit consumes 300 mW of electrical power, and the 23 thermal phase shifters (thermal efficiency of 28 mW/$\pi$) would cost around 812 mW at the worst case. Altogether, the photonic engine would demand roughly 1112 mW maximum.

### Thermal crosstalk

For configurability, the system contains 52 thermal tuners, making it quite sensitive to external and internal temperature fluctuations. In addition, the power dissipation of the transfer-printed laser (300 mW) and the modulator termination (80 mW at −2 V) make the thermal control even more challenging. Even though the sample is mounted on a temperature controller, it still drifts with ambient temperature. But when this is well controlled, the system shows a high stability and repeatability, which means that the different internal crosstalk contributions can be compensated by the on-chip tuners.

### Optical crosstalk

The chip has an integrated laser, but no optical isolator. This makes the laser cavities vulnerable to all reflections along the optical path. As an example, the used grating couplers have a reflection of around 1.6%. As these are not fully avoidable, all phase tuners will also affect the reflected light, introducing small perturbations to the laser cavity. However, the tunability of the system allows us to compensate for most of these. In our experiments, these effects were not a problem to realize the different demonstrations, but further characterization will be needed to develop robust compensation strategies.

### RF crosstalk

The RF packaging of our photonic engine is not perfect, resulting in RF crosstalk. The circuit board allows the RF signal to couple directly from the input connectors to the output connectors, bypassing the chip. Experimental measurements indicate that the RF crosstalk is approximately -60 dB. Because we did not boost the PD output with a transimpedance amplifier (TIA), their relatively weak signal is drowned in the direct RF crosstalk and cannot be retrieved. For the reported experiments, we made use of the optical ports to insert an off-chip EDFA (the only necessary optical device) to boost the modulated optical signal and then feed it back into the chip, or alternatively we used a separate off-chip detector. With a suitable TIA and even better RF isolation, these measures would not be necessary. Details of this characterization are shown in the Supplementary Information 3.5.

### Performance improvement

As discussed above, the main limitation of our photonic engine is the low RF signal readout from the on-chip PD and the unavoidable RF crosstalk, resulting in a low signal-to-noise ratio (SNR). This affects the performance of all demonstrations and necessitates the use of an off-chip EDFA.

To address these issues, the most effective solution is the integration of a proper TIA near the output of the on-chip PD. This could be realized through monolithic integration, micro-transfer printing, or surface-mount device (SMD) assembly with wire bonding. The addition of a TIA would enable reliable RF signal readout from the PD and significantly enhance the SNR. Moreover, RF wire bonding could help reduce crosstalk by minimizing electromagnetic radiation.

### Summary

By overcoming these bottlenecks, this silicon photonics-based engine can enable optical and microwave signal processing with all the key components. Its compact, low-power design highlights its potential for data centers, wireless communication, and microwave applications.

## Methods
### Silicon Chip Fabrication

The photonic chip was fabricated in the imec iSiPP50G silicon photonic platform on 200 mm wafers. The chip size is $1.3 \times 5$ mm$^2$ without grating couplers and $3.3 \times 5$ mm$^2$ with grating couplers. The chip layout is designed using IPKISS by Luceda Photonics.

### Transfer printing process

Transfer printing technology uses a stamp to pick up a prefabricated SOA coupon from a III-V source wafer and print it onto the target position of the silicon photonic sample (or wafer). In this process, SOAs are fabricated on a 2" wafer of InP epitaxial layer stack, grown by the metal-organic vapor-phase epitaxy (MOVPE) method at III-V Lab. A release layer is incorporated beneath the SOA device layer stack. After devices are patterned, the release layer is selectively etched, resulting in free-standing components held by tethers. A polydimethylsiloxane (PDMS) stamp is then laminated against these released devices, termed "coupons". When the stamp is rapidly pulled away, the coupons adhere due to strong bonding, break the tethers, transferring the devices to the stamp.

After pick-up, the stamp now carrying the device (either single or array), is aligned to the destination wafer using pattern recognition through the transparent PDMS stamp. The printing process entails laminating the stamp to the target wafer and retracting it slowly, using a shear force, ensuring the coupons adhere to the target wafer. To enhance coupon adhesion, an divinylsiloxane bisbenzocyclobutene (DVS-BCB) adhesion layer is used. After the process, one metallization step is necessary to link the transfer-printed components with the bondpads on the original silicon photonic sample[31].

On the imec iSiPP50G platform, a localized back-end opening (recess) is necessary to interface with the Si waveguide, permitting the seamless integration of III-V SOAs with Si structures. The 40 $\mu m$ wide III-V SOA measures 1 mm, including two 180 $\mu m$ adiabatic tapers to

enhance the coupling efficiency. Underneath the SOA, there's a continuous poly-Si/c-Si waveguide (with respective thicknesses of 160 nm and 220 nm) ensuring optimal optical coupling between the III-V device layer and the Si waveguide below it. Moreover, an added taper structure aids in channeling the optical mode to the 220 nm thick crystalline Si wire waveguide. Detailed information regarding the design and production of the III-V/Si SOAs can be found in[11], and more details can be seen in Supplementary Information 1.2.

## Optical, electrical, and RF Packaging
Fiber arrays are used for coupling the light in and out of chip. A fiber array is actively aligned by maximizing transmission through a shunt waveguide and then fixed in place on the processed sample using UV-curable epoxy. A 15 dB loss is measured for the reference waveguide ports, corresponding to a 7.5 dB loss per grating coupler. The use of edge couplers instead of grating couplers could significantly reduce the insertion loss of the fiber interfaces[9].

The 68 DC channels (heaters, tap monitors and grounds) and 3 RF ports (1 input, 2 outputs) are wirebonded to a high-speed printed circuit board (PCB), which for the high-speed RF ports shows a 3 dB loss at 40 GHz. More details are shown in the Supplementary Information 1.3. However, the modulator and the PD performance show that the wirebonding to the transmission line introduces a high loss and high RF crosstalk, which limits the maximum frequency that the full system can support to 25 GHz. A better RF packaging solution may relax these constrains and bring the performance up to the level of what we measured using RF probes: 33 GHz for the modulator and 50 GHz for the PDs.

## Electrical driving system
The transfer-printed SOA, the tap monitors and the on-chip PDs are driven by a Tektronix Keithley 2401. The heater-based optical phase shifters for tuning and configuration are driven by a PXI 6704 from National Instruments.

## Optical response measurement
No external laser is used to generate the different functions described above. The transmission spectrum for the O/O functionality was measured with an optical network analyzer (LUNA, OVA5000), which does contain a tunable laser, but which is only used for characterization purposes. The off-chip PD is a 42 GHz PD (Discovery LabBuddy DSC10H).

## Electrical response measurement
The E/E response is measured by a Keysight vector network analyzer(E8364B, 50 GHz). The RF signal source in Fig. 5b is a 40 GHz signal generator (Rohde & Schwarz SMR 40) and the electrical spectrum analyzer in Fig. 5b is a Keysight EXA signal analyzer (N9010A 44 GHz). The ESA used in Fig. 6b for the spectrum and phase noise measurement is an Anritsu MS2840A (26 GHz).

## Data availability
The data generated in this study have been deposited in the Figsure database [dx.doi.org/10.6084/m9.figshare.25035917].

## References

1. Yao, J. Microwave photonic systems. *J. Light. Technol.* **40**, 6595–6607 (2022).
2. Guan, Y. et al. Tera-sample-per-second arbitrary waveform generation in a synthetic dimension. *Commun. Phys.* **6**, 1–9 (2023).
3. Li, Z. et al. All-fiber optical nonreciprocity based on parity-time-symmetric Fabry-Perot resonators. *Commun. Phys.* **5**, 1–8 (2022).
4. Fandiño, J. S., Muñoz, P., Doménech, D. & Capmany, J. A monolithic integrated photonic microwave filter. *Nat. Photonics* **11**, 124–129 (2016).
5. Guo, X. et al. Versatile silicon microwave photonic spectral shaper. *APL Photonics* **6**, 36106 (2021).
6. Pérez-López, D. et al. General-purpose programmable photonic processor for advanced radiofrequency applications. *Nat. Commun.* **15**, 1–11 (2024).
7. Garrett, M. et al. Integrated microwave photonic notch filter using a heterogeneously integrated Brillouin and active-silicon photonic circuit. *Nat. Commun.* **14**, 1–9 (2023).
8. Feng, H. et al. Integrated lithium niobate microwave photonic processing engine. *Nature* **627**, 80–87 (2024).
9. Ferraro, F. et al. Imec silicon photonics platforms: performance overview and roadmap. **12429**, 22–28 https://doi.org/10.1117/12.2650579 (2023).
10. Zhang, J. et al. Micro-transfer printing InP C-band SOAs on advanced silicon photonics platform for lossless MZI switch fabrics and high-speed integrated transmitters. *Opt. Express* **31**, 42807–42821 (2023).
11. Soltanian, E. et al. Micro-transfer-printed narrow-linewidth III-V-on-Si double laser structure with a combined 110 nm tuning range. *Opt. Express* **30**, 39329–39339 (2022).
12. Li, Y., Li, L., Tian, B., Roelkens, G. & Baets, R. G. Reflectionless tilted grating couplers with improved coupling efficiency based on a silicon overlay. *IEEE Photonics Technol. Lett.* **25**, 1195–1198 (2013).
13. Van Gasse, K. et al. III-V-on-silicon photonic transceivers for radio-over-fiber links. *J. Light. Technol.* **36**, 4438–4444 (2018).
14. Tao, Y. et al. Fully on-chip microwave photonic instantaneous frequency measurement system. *Laser Photonics Rev.* **16**, 2200158 (2022).
15. Porzi, C. et al. Photonic integrated microwave phase shifter up to the mm-wave band with fast response time in silicon-on-insulator technology. *J. Light. Technol.* **36**, 4494–4500 (2018).
16. Liu, W. et al. A fully reconfigurable photonic integrated signal processor. *Nat. Photonics 2016 10:3* **10**, 190–195 (2016).
17. Chrostowski, L. et al. Silicon photonic resonator sensors and devices. https://doi.org/10.1117/12.916860 **8236**, 387–402 (2012).
18. Deng, H., Zhang, W. & Yao, J. High-speed and high-resolution interrogation of a silicon photonic microdisk sensor based on microwave photonic filtering. *J. Light. Technol.* **36**, 4243–4249 (2018).
19. Wang, M., Ribero, A., Xing, Y. & Bogaerts, W. Tolerant, broadband tunable 2 × 2 coupler circuit. *Opt. Express* **28**, 5555 (2020).
20. Madsen, C. K. & Zhao, J. H. Optical filter design and analysis. Wiley Series in Microwave and Optical Engineering (John Wiley & Sons, Inc., New York, 1999).
21. Luo, L.-W. et al. High bandwidth on-chip silicon photonic interleaver. *Opt. Express* **18**, 23079–23087 (2010).
22. Deng, H. & Bogaerts, W. Pure phase modulation based on a silicon plasma dispersion modulator. *Opt. Express* **27**, 27191 (2019).
23. Yao, J. Microwave photonics. *J. Light. Technol.* **27**, 314–335 (2009).
24. Zhang, W. et al. A system-on-chip microwave photonic processor solves dynamic RF interference in real time with picosecond latency. *Light Sci. Appl.* **13**, 1–12 (2024).
25. Pérez-López, D., Gutiérrez, A. & Capmany, J. Silicon nitride programmable photonic processor with folded heaters. *Opt. Express* **29**, 9043–9059 (2021).
26. Catalá-Lahoz C., Pérez-López D., Huy-Ho T. & Capmany J. Self-configuring programmable silicon photonic filter for integrated microwave photonic processors. *APL Photonics* **8**, 116103 (2023).
27. Zhang, W. & Yao, J. Silicon photonic integrated optoelectronic oscillator for frequency-tunable microwave generation. *J. Light. Technol.* **36**, 4655–4663 (2018).

28. Tsokos, C. et al. True time delay optical beamforming network based on hybrid InP-Silicon nitride integration. *J. Light. Technol.* **39**, 5845–5854 (2021).
29. Daulay, O. et al. Ultrahigh dynamic range and low noise figure programmable integrated microwave photonic filter. *Nat. Commun.* **13**, 1–8 (2022).
30. Zand, I. & Bogaerts, W. Effects of coupling and phase imperfections in programmable photonic hexagonal waveguide meshes. *Photonics Res.* **8**, 211 (2020).
31. Roelkens, G. et al. Micro-Transfer Printing for Heterogeneous Si Photonic Integrated Circuits. *IEEE J. Sel. Top. Quant. Electron.* **29**, 8200414 (2023).
32. Zhang, W. & Yao, J. Photonic integrated field-programmable disk array signal processor. *Nat. Commun.* **11**, 1–9 (2020).
33. Xie, Y. et al. Low-loss chip-scale programmable silicon photonic processor. *Opto-Electron. Adv.* **6**, 220030–1 (2022).

## Author contributions

H.D. and W.B. conceived the idea of the project. H.D. and J.Z. simulated and designed the whole system and laid out the mask. H.D. performed the experimental characterizations and analysis. E.S. helped with the transfer printing process. X.C. helped with the mask layout. C.P. helped with the chip post-processing. N.V., D.N., J.R., and J.D. provided the SOA coupon fabrication. N.S. and G.T. helped with the OEO characterization. H.D., E.S., and W.B. wrote the paper. G.R. and W.B. supervised the project. All authors commented on the manuscript.

## Competing interests

The authors declare no competing interests.

## Additional information

**Supplementary information** The online version contains supplementary material available at https://doi.org/10.1038/s41467-025-60100-0.

**Correspondence** and requests for materials should be addressed to Hong Deng or Wim Bogaerts.

**Peer review information** *Nature Communications* thanks David Marpaung and the other anonymous reviewer(s) for their contribution to the peer review of this work. A peer review file is available.

**Reprints and permissions information** is available at http://www.nature.com/reprints

**Publisher's note** Springer Nature remains neutral with regard to jurisdictional claims in published maps and institutional affiliations.